HHS Public Access

Author manuscript

Environ Toxicol Chem. Author manuscript; available in PMC 2016 January 14.

Published in final edited form as:

Environ Toxicol Chem. 2012 January ; 31(1): 93–99. doi:10.1002/etc.708.

Solubility of nano-zinc oxide in environmentally and biologically important matrices

Robert B. Reed[†], **David A. Ladner**[‡], **Christopher P. Higgins**[§], **Paul Westerhoff**[‖], and **James F. Ranville**[*,†]

[†]Department of Chemistry and Geochemistry, Colorado School of Mines, Golden, Colorado, USA

[‡]Department of Environmental Engineering and Earth Sciences, Clemson University, Anderson, South Carolina, USA

[§]Division of Environmental Science and Engineering, Colorado School of Mines, Golden, Colorado, USA

[‖]School of Sustainable Engineering and the Built Environment, Arizona State University, Tempe, Arizona, USA

Abstract

Increasing manufacture and use of engineered nanoparticles (NPs) is leading to a greater probability for release of ENPs into the environment and exposure to organisms. In particular, zinc oxide (ZnO) is toxic, although it is unclear whether this toxicity is due to the zinc oxide nanoparticles (ZnO), dissolution to Zn^{2+}, or some combination thereof. The goal of this study was to determine the relative solubilites of both commercially available and in-house synthesized ZnO in matrices used for environmental fate and transport or biological toxicity studies. Dissolution of ZnO was observed in nanopure water (7.18– 7.40 mg/L dissolved Zn, as measured by filtration) and Roswell Park Memorial Institute medium (RPMI-1640) (~5 mg/L), but much more dissolution was observed in Dulbecco's Modified Eagle's Medium (DMEM), where the dissolved Zn concentration exceeded 34 mg/L. Moderately hard water exhibited low zinc solubility, likely due to precipitation of a zinc carbonate solid phase. Precipitation of a zinc-containing solid phase in RPMI also appeared to limit zinc solubility. Equilibrium conditions with respect to ZnO solubility were not apparent in these matrices, even after more than 1,000 h of dissolution. These results suggest that solution chemistry exerts a strong influence on ZnO dissolution and can result in limits on zinc solubility due to precipitation of less soluble solid phases.

Keywords

Nanoparticle dissolution; Zinc ion release; Zinc solid precipitation; Cell culture media

Corresponding Author: James F. Ranville, Colorado School of Mines, Department of Chemistry and Geochemistry, 1500 Illinois St., Golden, CO 80401, Phone: (303) 273-3004, Fax: (303) 273-3629, jranvill@mines.edu.

Introduction

Zinc oxide nanoparticles (ZnO NPs) have been used in a variety of products and applications such as semiconductors, catalysts, and paints and increasingly are found in consumer products such as sunscreen due to ZnO's strong ultraviolet absorption properties [1]. Increased production and use of ZnO suggests increased exposure potential for humans and other organisms. Although studies quantifying exposures of humans to engineered NPs are scarce, it is likely that increased industrial production will lead to human contact and exposures (dermal, inhalational, and ingestion) [2]. These routes of exposure are well studied for various particles previously termed "submicron" in size [3–5], many of which are in the nanometer size regime. These previous risk assessments provide a starting point for analyzing risks associated with engineered NPs, but further studies are needed due to their novel properties.

Release of NPs into the environment (e.g., through wastewater treatment plant effluent) should increase ecosystem exposure, though this is difficult to quantify. Modeling efforts indicate that environmental ZnO concentrations may currently be high enough (0.3 μg/L in the US; 0.432 μg/L in Europe) in wastewater treatment plant effluent to pose a toxicological threat to aquatic organisms [6]. Monitoring transformations in relevant matrices [7–9] enables an evaluation as to how long particles may persist in environmental or biological systems. Zinc-oxide toxicity to animals has been studied using in vitro tests [10–14] and in vivo tests [15–21]. When compared to other NPs, ZnO has often been found to be among the most toxic [12,20,22]. Although ZnO NPs have been reported to have greater toxicity than dissolved Zn^{2+} alone [14], the general consensus is that these particles dissolve relatively quickly and that the Zn^{2+} ionis the primary source of toxicity [11,15,20]. A recent toxicology study by Poynton et al. [23] suggested that both ZnO NPs and Zn^{2+} are toxic, but have different modes of action. George et al. [24] showed that iron-doping of ZnO NPs led to reduced dissolution and thereby decreased cytotoxicity, suggesting the possibility for manufacturing safer nanomaterials. Another study, however, examining the effects of iron-doped ZnO on bacterial toxicity [25] showed that water chemistry influenced toxicity far more than doping.

With increasing human exposure to engineered NPs, data reflecting their behavior in systems at physiological temperature and pH become more valuable. As Zn^{2+} released by ZnO NPs is generally accepted as an important contributor to ZnO toxicity, it is crucial to quantify the amount generated from a given dose of NPs. In the present study, we compare dissolution of several ZnO NPs with bulk ZnO and a dissolved Zn reference ($ZnCl_2$) in biologically and environmentally relevant matrices. While previous studies have measured the amount of dissolved zinc released by ZnO NPs in simple solutions [15] and in cell culture media used for toxicity studies [14], to our knowledge, the present study is the first to quantify ZnO dissolution with multiple particle types and sizes in a variety of matrices and temperatures. The goal of the present study was to examine how the extent and rate of ZnO dissolution varies with matrix, temperature, and particle source. In addition, a methodological comparison between 0.02-μm pore syringe filters and centrifugal ultrafilters was made to determine if one was more effective than the other at separating particulate from dissolved species.

Experiments

Materials

Zinc oxide particles used include a bulk powder (Alfa Aesar, 99.99% purity by metals basis) and three different aqueous suspensions (Alfa Aesar 44904, 45409, and 45588; manufacturer did not provide purity). A fourth, in powder form, was obtained from the University of California, Los Angeles.as a reference material for toxicology studies being performed concurrently by a consortium of research groups at several institutions in the United States. An ionic zinc source ($ZnCl_2$, reagent grade, Fischer Scientific) was used as a dissolved zinc control.

Characterization of NPs

A Zetasizer Nano ZS (Malvern) was used to determine the hydrodynamic diameter by dynamic light scattering. Samples of 100 mg/L ZnO dispersed in nanopure water (Barnstead Nanopure Diamond, APS Water) were analyzed in triplicate. The mean diameter ±standard deviation is provided for each particle in Table 1. Zeta potential measurements were also performed using the Malvern Zetasizer Nano ZS on 100 mg/L ZnO solutions in nanopure water. The measurements were taken in duplicate and reported as mean ±standard deviation. The pH of the solutions for the zeta potential determinations was measured to be approximately eight.

X-ray diffraction (XRD) with a Philips X'pert Pro Diffractometer (PANalytical) was performed to confirm the NPs' chemical identity as ZnO. The solid powders were placed in sample holders and analyzed with Cu K_α radiation at 2θ angles from 5° to 90°. The aqueous suspensions were prepared for analysis by placing a few drops of solution onto glass microscope slides and drying overnight to produce a solid ZnO sample. These were analyzed by the same method as the powders. Analysis of Zn precipitate formed in Roswell Park Memorial Institute-1640 (RPMI-1640) was also performed by XRD. A solution of approximately 80 mg/L Zn from aqueous $ZnCl_2$ stock solution in RPMI was centrifuged at 4,000 rpm for 40 min to obtain precipitate. This was dried at 100°C and ground into a powder for XRD analysis.

A JSM-7000F (JEOL) field mission scanning electron microscope was used to image the particles for information on particle size distribution and particle morphology. The samples were analyzed at 2.0 kV and imaged at 45–55,000× magnification, except the larger bulk ZnO, which was imaged at 25,000×. The samples were prepared as 100 mg/L ZnO solutions, spotted, and vacuum dried on a 47mm 0.1 μm-pore size polycarbonate filter membrane (Nucleopore). This was then fixed to a sample mount with carbon tape and gold sputter-coated prior to analysis. This instrument was used in concert with energy dispersive X-ray spectroscopy (EDAX Genesis Energy) to determine the elemental composition of precipitates formed in moderately hard water and RPMI. Zinc precipitates from moderately hard water and RPMI were collected as described for XRD analysis and fixed to carbon tape on a sample mount for analysis. Blank solutions of moderately hard water and RPMI (no Zn added) were centrifuged under the same conditions to ensure any precipitate observed was

not solely a product of the matrix. No precipitates were observed in the blanks. The results of characterization are shown in Table 1.

Dissolution experiments

A long-term dissolution study was performed to investigate the equilibrium solubility of Zn^{2+} from dissolving 100 mg/L solutions in four matrices: nanopure water, EPA moderately hard water [26], Dulbecco's Modified Eagle's Medium (DMEM, D5796, Sigma) and RPMI-1640 (R8758, Sigma) cell culture media. These media were chosen because of their use in toxicity studies and their differing constituents, which may control solubility, particularly phosphate (0.906 mM in DMEM and 5.64 mM in RPMI; both buffered at pH 7.3; see Supplemental Data Table S1 for full constituent list). Additional matrices were created by adding 2 mg/ml bovine serum albumin (BSA) to DMEM and RPMI solutions to investigate possible effects of protein presence on dissolution. ZnO samples were prepared in 500 ml high-density polyethylene bottles, which were first placed in a 5% HNO_3 (Fischer Scientific) acid bath overnight and rinsed thoroughly with nanopure water to prevent residual zinc contamination. Preparation and filtration of solutions were performed in a filtered-air laminar flow hood to prevent both zinc and microbial contamination. Care was taken to avoid touching bottle interiors while sampling; samples were poured directly into syringes, with no pipet tips being placed into bottles. No microbial growth was visible over the course of the experiment. All bottles were sealed at all times except when sampling. Between subsequent time points, all bottles were placed vertically on a shaker table running at approximately 80 rpm to prevent settling of NPs.

Filtering and analyzing a sample of each matrix prior to adding ZnO particles determined the background levels of zinc in the matrices. Adding ZnO to a bottle was followed by inversion to mix the solution and immediate collection and filtration of a subsample to obtain a t = 0 h value for dissolved Zn^{2+}. Syringe filters with 0.02 μm pores (Anotop 25mm, Whatman) were used to separate dissolved Zn^{2+} from ZnO NPs. Dissolved Zn^{2+} concentration was determined by inductively coupled plasma mass spectrometry (Perkin Elmer Elan 6100) and inductively coupled plasma atomic emission spectroscopy (ICP-AES, Perkin Elmer Optima 5300 DV) after acidification to 2% nitric acid. Mixed-metal standards were used for instrument calibration prior to each analysis, and check standards were analyzed at the beginning and end of each run as well as after every ten samples for quality control. To calculate dissolution rates, long-term dissolution data for dissolved Zn versus time were fit to linear models of the form $[Zn_{dissolved}]$ = slope × time + intercept using OriginPro 8.1.

In addition to 100 mg/L ZnO, a particle concentration more relevant to toxicity exposure tests [12,16,22,27,28], 10 mg/L, was prepared for short-term dissolution studies in cell culture media. The effects of temperature on dissolution were also examined. Solutions of DMEM and RPMI were maintained at room temperature (20°C) and human body temperature (37°C) during dissolution of 100 mg/L and 10 mg/L ZnO (Alfa Aesar 44904 and consortium) and $ZnCl_2$. After adding the zinc, the solution was inverted twice and a subsample collected and filtered immediately with Anotop 0.02-μm pore filters. The solutions were stored overnight on shaker tables at both room temperature and in an

incubator at 37°C and filtered again at 24 h. Zinc concentration in the filtrate was determined by ICP-AES (Perkin Elmer Optima 5300 DV).

Equilibrium modeling

Chemical equilibrium modeling using Visual MINTEQ Version 3.0 was performed to determine if Zn-containing precipitates would be formed after dissolution to Zn^{2+} in moderately hard water and RPMI. The inorganic constituents of each matrix were entered into the model and each used to calculate saturation indices in the presence of 8 and 80 mg/L Zn^{2+} (for 10 and 100 mg/L ZnO, respectively).

Ultrafiltration experiment

Complementary short-term dissolution experiments were performed using centrifugal ultrafilters (Amicon Ultra, Millipore) to separate particles from ionic Zn^{2+}. Alfa Aesar 44904 and consortium NPs were used to compare separation effectiveness of the 0.02-μm pore syringe and centrifugal filters. For centrifugal filtration experiments, solutions were made in nanopure water, EPA moderately hard water, DMEM, and RPMI at a concentration of 10 mg/L ZnO and tested separately with 100 kDa membranes. $ZnCl_2$ solutions at a concentration of 8.37 mg/L (0.12 mM Zn, the same as the solutions) were made in the same matrices as a test for Zn precipitation. Ten milliliters of suspension or $ZnCl_2$ solution were added to the filtration device and centrifuged for 30 min at 5,000 *g*. The permeate was collected, weighed, and saved for analysis. Nanopure water was then added to the concentrate side of the filtration device and shaken by hand to resuspend NPs collected on the membrane. The resuspended concentrate was weighed and analyzed at the same time as the permeate. Analysis of dissolved zinc was performed by ICP-AES (iCAP 6300 Duo, Thermo) after acidification with 3% nitric acid. Because resuspension of the NPs from the centrifugal filter membrane allowed a systematic calculation of recovery, the rejection data complimented the filtrate concentration data. This approach for obtaining a mass balance was not possible with the sealed syringe filters, where sample handling for recovery determination was not feasible. In addition, five different ultrafilter molecular weight cutoffs (3, 10, 30, 50, and 100 kDa) were compared for separation effectiveness using Alfa Aesar 44904 and consortium NPs.

Results and Discussion

Dissolution in nanopure and moderately hard water

Quantification of Zn^{2+} following 0.02-μm pore filtration showed similar degrees of dissolution for each of the three Alfa Aesar ZnO particles in nanopure water, with all three solutions exceeding 7 mg/L of Zn^{2+} after 810 h (Figure 1a). Comparing rates of particle dissolution, the bulk ZnO (5.56 $\mu g\ L^{-1}\ hr^{-1}$) was slower to dissolve than all three NPs (7.43 to 8.48 $\mu g\ L^{-1}\ hr^{-1}$) (see Supplemental Data Tables S2–S5). This could be attributed to a greater specific surface area of the smaller NPs relative to the larger bulk-phase particles. In moderately hard water (Figure 1b) dissolution of the bulk and two of the NPs was minimal. Interestingly, the smallest particle (Alfa Aesar 45409, 40 nm) showed dissolution to 2.24 mg/L Zn^{2+} after 810 h in moderately hard water, also suggesting a specific surface area

effect. A relatively small amount of dissolution in moderately hard water suggests that ZnO NPs may persist in the environment once released.

To explain the observed differences in the amount of apparent dissolution, equilibrium chemical modeling was conducted to determine the potential for zinc that dissolved from NPs to reprecipitate. Modeling of dissolved zinc in moderately hard water by Visual MINTEQ suggests that dissolution of ZnO NPs results in oversaturation of Zn^{2+} with respect to a solid phase of hydrozincite, $Zn_5(CO_3)_2(OH)_6$,with possible additional phases of $ZnCO_3$ and ZnO (Supplemental Data, Table S6).

Atomic weight percentages by energy dispersive X-ray spectroscopy (EDX) analysis of precipitates collected from moderately hard water after adding $ZnCl_2$ supported this prediction (Supplemental Data Figure S1), although the small mass of precipitate obtained did not allow for further confirmation by XRD analysis. Zn solid phase changes from NPs have been reported; spontaneous formation of $ZnCO_3$ nanowire species from ZnO nanowires after exposure to ambient air levels of water and CO_2 was observed [29]. Formation of precipitates larger than 20 nm in particle diameter would be rejected by the largest filter pores (0.02 μm) used in this study and would not contribute to dissolved zinc concentration. Also, solid precipitates of $CaCO_3$ large enough to be rejected by filtration may adsorb zinc ions [30] and effectively remove them from solution as well.

Dissolution in cell culture media

In DMEM and RPMI cell culture media, a higher extent of dissolution was observed when compared to nanopure or moderately hard water. In DMEM, an apparent instantaneous dissolution was observed for all NPs, with a slow, subsequent increase in dissolved Zn (Figure 2a). Dissolved zinc from bulk ZnO increased quickly during the first 24 h and remained relatively constant before reaching an eventual maximum of 8.45 mg/L. The dissolved zinc resulting from dissolution of Alfa Aesar 44904 showed an immediate Zn^{2+} solubility greater than 10 mg/L and eventually climbed to 34.2 mg/L at 1,446 h. In this experiment, an excess of ZnO NPs was added to the cell culture media (100 mg/L). However, the fast dissolution to reach a dissolved Zn concentration greater than 10 mg/L suggests that lower starting concentrations may completely dissolve to Zn^{2+} in this medium.

A greater extent of dissolution (13.6 mg/L) was observed for the bulk ZnO in the presence of BSA. Particle-protein complexes that create a protein corona on the particle surface have been studied [31–34] and the extent of protein complexation may greatly affect how these particles interact with biological systems. These coronae could affect the stability of the particles and cause a change in their dissolution. Although BSA-containing solutions quickly clogged the filter pores in this experiment, some amount of BSA (8 nm for an average monomer [35]) could be passed through the 0.02-μm pore filters with bound zinc [36], increasing the zinc concentration in the filtrate.

In RPMI, a smaller difference in dissolved zinc between bulk- and NP-containing solutions was observed (Figure 2b). The nanoparticulate ZnO appears to dissolve more than the bulk, but the difference between the phases is not as pronounced as in DMEM. A lower overall solubility for both phases was observed as well, with the nano ZnO reaching 4.66 mg/L at

1,446 h. Modeling by Visual MINTEQ predicted $Zn_3(PO_4)_2 \cdot 4H_2O$ to precipitate in RPMI (Supplemental Data Table S6; using inorganic substituents for modeling only; RPMI also contains vitamins not included in Visual MINTEQ's library). Analysis of collected precipitates by EDX showed atomic ratios that agreed with this prediction (Supplemental Data Figure S2). A greater amount of solid precipitated in RPMI than in moderately hard water, and XRD analysis was performed to confirm the crystal structure with the closest library match being a zinc phosphate hydrate phase. A higher amount of phosphate is contained in RPMI than in DMEM (Supplemental Data Table S1), which may account for much of the difference in solubility. Although we did not observe precipitates forming in NP-containing solutions themselves due to the large quantity of NPs already present, it can be inferred from precipitate analysis after addition of $ZnCl_2$ to these matrices that Zn^{2+} released by dissolving NPs in a given matrix may simply precipitate in another form and not be present as either NPs or dissolved Zn.

This long-term dissolution of ZnO NPs in cell culture media could be useful in predicting behavior in some biological systems. While ingestion and dermal exposures occur over shorter time scales, particles lodging in the lungs [37] can have long-term effects. The observed solubility of ZnO NPs in simulated biological matrices suggests these particles could create very high local concentrations of dissolved Zn if lodged in the lungs. In addition, inhaled TiO_2 NPs have been found to be transported from the lungs to compartments such as the liver, heart, and nervous system [38]. It is not known if ZnO NPs would persist in this environment long enough to exhibit similar transport behavior due to their higher solubility, but exposure to ZnO would likely result in elevated dissolved Zn concentrations.

Effect of temperature on dissolution

For 100 mg/L ZnO samples in DMEM and RPMI, a consistent trend toward less zinc solubility was observed at 37°C when compared to 20°C (Figure 3). A very consistent decrease in zinc solubility at 37°C was observed in DMEM, with dissolved Zn concentrations around 6 to 7 mg/L for both particles at 0 and 24 h, as opposed to ~12 to 13 mg/L at 20°C. As the enthalpy of ZnO dissolution is negative [39], it is expected that an increased temperature would result in lower Zn^{2+} solubility. As observed in long-term experiments, immediate dissolution of ZnO in RPMI to ~2 mg/L occurred, and this was still evident after 24 h at 20°C for ZnO NPs. The difference in zinc solubility between temperatures in RPMI is not as large as in DMEM, but a slight decrease was observed for all NPs at 37°C. For $ZnCl_2$ in DMEM, a similar constancy at 0 and 24 h and difference in solubility is seen between 20°C and 37°C as in the solutions; however, the concentrations are higher at approximately 25 and 17 mg/L, respectively.

At 10 mg/L ZnO, instantaneous dissolution behavior was also observed for the Alfa Aesar (Figure 4). At this concentration, however, the consortium was not observed to undergo the same immediate dissolution in DMEM as it exhibited at 100 mg/L. This could be due to a smaller degree of specific surface area for the consortium relative to the Alfa Aesar. The consortium ZnO is a powder that tends to remain as large aggregates of NPs in solution, reducing its available surface area, while the Alfa Aesar is well dispersed in aqueous

solution. Although aggregation may affect dissolution rates, the potential for this effect was not a focus of the present study.

Although the present study was not designed to address the toxicity of the NPs examined, it has implications for toxicity research. In DMEM, the relatively high zinc solubility and instantaneous dissolution of some ZnO NPs raises questions about the ability to assess toxicity of these NPs when dosed in this medium. If this medium or another with similar zinc solubility was used in toxicity studies, it could be incorrectly concluded that the NPs are responsible for any observed toxic effect, even though no actual exposure occurs due to their dissolution. Therefore, caution should be exercised in attributing toxicity to NPs if the solubility of Zn in the matrices used is not well known; indeed, solution chemistry appears to play a major role in the dissolution of ZnO NPs. In addition, particle type also appears to affect solubility. This is evidenced by the differences in behavior between bulk phase and nanoparticulate ZnO; ZnO NPs from different sources; and between NPs of different sizes. Solution temperature also had an effect on dissolution in cell culture media, demonstrating that ZnO NPs may behave differently at human body temperature as opposed to room temperature.

Separation of zinc species by ultrafiltration

In an attempt to provide increased resolution of size and develop alternative filtration practices for NPs in biological testing, centrifugal ultrafiltration of samples was conducted, and the results were compared against 0.02-μm pore filtration. Syringe and centrifugal filters have been compared for quantification of dissolved Pb^{2+} released from PbS aggregates with similar effectiveness [40]. Overall, ZnO dissolution in the same four matrices (nanopure water, moderately hard water, DMEM, and RPMI) as determined by centrifugal filtration experiments exhibited similar behavior as when filtered by 0.02-μm pore filters (Figure 5).

Furthermore, all five ultrafilter sizes (3–100 kDa) behaved similarly (Supplemental Data Fig. S4), suggesting they all adequately discriminated between nanoparticulate and dissolved zinc. In the ultrafiltration experiments, the feed concentration was measured (and plotted in Figure 5 as the sum of dissolved and particulate zinc) for each replicate. The centrifugal filtration takes approximately 30 min, so a t = 0 data point is more likely to be between 0.5 and 1 h. This additional time could allow for a greater amount of dissolution relative to syringe filtration, where the first filtrate is collected approximately one minute after suspension of NPs. Compared with nanopure water, NPs in moderately hard water showed less dissolution after 24 h—0.69 mg/L Zn for Alfa Aesar 44904 and 1.1 mg/L for the consortium particle. Moderately hard water also prevented the soluble zinc source ($ZnCl_2$) from passing through the membrane, again indicating formation of filterable precipitates from dissolved zinc. Lower permeate Zn concentrations from the filtered $ZnCl_2$ solution after 24 h suggests continued precipitation over this time period. The culture fluids RPMI and DMEM again showed an immediate dissolution of NPs and little increase past that point after 24 h. The bulk of the data suggests relatively stable solubility maxima for aqueous zinc species in these matrices. However, the increase in solubility in DMEM after 600 h may indicate that a more complex process may control zinc solubility. These studies indicate that small pore filters and ultrafilters provide comparable data for ZnO NPs related

to dissolution and potential reprecipitation. The results of this study suggest that the solubility of NPs may be highly variable and dependent on the matrix in which they are suspended. Dissolution and reprecipitation of soluble particles should be considered when attempting to ascertain the toxicity or environmental fate of engineered NPs.

Supplementary Material

Refer to Web version on PubMed Central for supplementary material.

Acknowledgments

This work was supported by the National Institute of Health (NIH) Grand Opportunities (RC2) program through National Institute of Environmental Health Sciences grant DE-FG02-08ER64613. ZnO NPs were synthesized for use by the NIH consortium at the University of California, Los Angeles. Special thanks to P. Brucker, D. Hietala, S. Bandrowsky, F. Lin, and J. Chandler.

References

1. Herzog B, Mongiat S, Deshayes C, Neuhaus M, Sommer K, Mantler A. In vivo and in vitro assessment of UVA protection by sunscreen formulations containing either butyl methoxy dibenzoyl methane, methylene bis-benzotriazolyl tetramethylbutylphenol, or microfine ZnO. Int J Cosmet Sci. 2002; 24:170–185. [PubMed: 18498509]
2. Maynard A. Airborne nanostructured particles and occupational health. J Nanopart Res. 2005; 7(6): 587–614.
3. Anderson KR, Avol EL, Edwards SA, Shamoo DA, Peng RC, Linn WS, Hackney JD. Controlled exposures of volunteers to respirable carbon and sulfuric acid aerosols. J Air Waste Manage Assoc. 1992; 42:770–776. [PubMed: 1637548]
4. Avol EL, Linn WS, Whynot JD, Anderson KR, Shamoo DA, Valencia LM, Little DE, Hackney JD. Respiratory dose-response study of normal and asthmatic volunteers exposed to sulfuric acid aerosol in the sub-micrometer size range. Toxicol Ind Health. 1988; 4:173–184. [PubMed: 3051519]
5. Stephenson D. Workplace exposure to submicron particle mass and number concentrations from manual arc welding of carbon steel. American Industrial Hygiene Association. 2003; 64:6.
6. Gottschalk F, Sonderer T, Scholz RW, Nowack B. Modeled environmental concentrations of engineered nanomaterials (TiO2, ZnO, Ag, CNT, Fullerenes) for different regions. Environ Sci Technol. 2009; 43:9216–9222. [PubMed: 20000512]
7. Metz KM, Mangham AN, Bierman MJ, Jin S, Hamers RJ, Pedersen JA. Engineered nanomaterial transformation under oxidative environmental conditions: development of an in vitro biomimetic assay. Environ Sci Technol. 2009; 43:1598–1604. [PubMed: 19350941]
8. Scheckel KG, Luxton TP, El Badawy AM, Impellitteri CA, Tolaymat TM. Synchrotron speciation of silver and zinc oxide nanoparticles aged in a kaolin suspension. Environ Sci Technol. 2010; 44:1307–1312. [PubMed: 20078035]
9. Zhang H, Gilbert B, Huang F, Banfield JF. Water-driven structure transformation in nanoparticles at room temperature. Nature. 2003; 424:1025–1029. [PubMed: 12944961]
10. Xia T, Kovochich M, Liong M, Madler L, Gilbert B, Shi HB, Yeh JI, Zink JI, Nel AE. Comparison of the mechanism of toxicity of zinc oxide and cerium oxide nanoparticles based on dissolution and oxidative stress properties. ACS Nano. 2008; 2:2121–2134. [PubMed: 19206459]
11. Kasemets K, Ivask A, Dubourguier HC, Kahru A. Toxicity of nanoparticles of ZnO, CuO and TiO2 to yeast *Saccharomyces cerevisiae*. Toxicol In Vitro. 2009; 23:1116–1122. [PubMed: 19486936]
12. Brunner TJ, Wick P, Manser P, Spohn P, Grass RN, Limbach LK, Bruinink A, Stark WJ. In vitro cytotoxicity of oxide nanoparticles: Comparison to asbestos, silica, and the effect of particle solubility. Environ Sci Technol. 2006; 40:4374–4381. [PubMed: 16903273]

13. Hu X, Cook S, Wang P, Hwang HM. In vitro evaluation of cytotoxicity of engineered metal oxide nanoparticles. Sci Total Environ. 2009; 407:3070–3072. [PubMed: 19215968]
14. Wu B, Wang Y, Lee YH, Horst A, Wang ZP, Chen DR, Sureshkumar R, Tang YJJ. Comparative eco-toxicities of nano-ZnO particles under aquatic and aerosol exposure modes. Environ Sci Technol. 2010; 44:1484–1489. [PubMed: 20102184]
15. Franklin NM, Rogers NJ, Apte SC, Batley GE, Gadd GE, Casey PS. Comparative toxicity of nanoparticulate ZnO, bulk ZnO, and ZnCl2 to a freshwater microalga (*Pseudokirchneriella subcapitata*): The importance of particle solubility. Environ Sci Technol. 2007; 41:8484–8490. [PubMed: 18200883]
16. Heinlaan M, Ivask A, Blinova I, Dubourguier HC, Kahru A. Toxicity of nanosized and bulk ZnO, CuO and TiO2 to bacteria *Vibrio fischeri* and crustaceans *Daphnia magna* and *Thamnocephalus platyurus*. Chemosphere. 2008; 71:1308–1316. [PubMed: 18194809]
17. Ma H, Bertsch PM, Glenn TC, Kabengi NJ, Williams PL. Toxicity of manufactured zinc oxide nanoparticles in the nematode *Caenorhabditis elegans*. Environ Toxicol Chem. 2009; 28:1324–1330. [PubMed: 19192952]
18. Wang B, Feng WY, Wang M, Wang TC, Gu YQ, Zhu MT, Ouyang H, Shi JW, Zhang F, Zhao YL, Chai ZF, Wang HF, Wang J. Acute toxicological impact of nano- and submicro-scaled zinc oxide powder on healthy adult mice. J Nanopart Res. 2008; 10:263–276.
19. Wong SWY, Leung PTY, Djurisic AB, Leung KMY. Toxicities of nano zinc oxide to five marine organisms: influences of aggregate size and ion solubility. Anal Bioanal Chem. 2010; 396:609–618. [PubMed: 19902187]
20. Aruoja V, Dubourguier HC, Kasemets K, Kahru A. Toxicity of nanoparticles of CuO, ZnO and TiO2 to microalgae *Pseudokirchneriella subcapitata*. Sci Total Environ. 2009; 407:1461–1468. [PubMed: 19038417]
21. Zhu X, Wang J, Zhang X, Chang Y, Chen Y. The impact of ZnO nanoparticle aggregates on the embryonic development of zebrafish (*Danio rerio*). Nanotechnology. 2009; 20:195103. [PubMed: 19420631]
22. Adams LK, Lyon DY, Alvarez PJ. Comparative eco-toxicity of nanoscale TiO2, SiO2, and ZnO water suspensions. Water Res. 2006; 40:3527–3532. [PubMed: 17011015]
23. Poynton HC, Lazorchak JM, Impellitteri CA, Smith ME, Rogers K, Patra M, Hammer KA, Allen HJ, Vulpe CD. Differential gene expression in *Daphnia magna* suggests distinct modes of action and bioavailability for ZnO nanoparticles and Zn ions. Environ Sci Technol. 2011; 45:762–768. [PubMed: 21142172]
24. George S, Pokhrel S, Xia T, Gilbert B, Ji Z, Schowalter M, Rosenauer A, Damoiseaux R, Bradley KA, Madler L, Nel AE. Use of a rapid cytotoxicity screening approach to engineer a safer zinc oxide nanoparticle through iron doping. ACS Nano. 2010; 4:15–29. [PubMed: 20043640]
25. Li M, Pokhrel S, Jin X, Madler L, Damoiseaux R, Hoek EM. Stability, bioavailability, and bacterial toxicity of ZnO and iron-doped ZnO nanoparticles in aquatic media. Environ Sci Technol. 2011; 45:755–761. [PubMed: 21133426]
26. U.S. Environmental Protection Agency. Methods for measuring the acute toxicity of effluents and receiving waters to freshwater and marine organisms. 5. Washington, DC: 2010. EPA 821-R-02–012 Analytical Methods Manual
27. Lin DH, Xing BS. Root uptake and phytotoxicity of ZnO nanoparticles. Environ Sci Technol. 2008; 42:5580–5585. [PubMed: 18754479]
28. Heng BC, Zhao XX, Xiong SJ, Ng KW, Boey FYC, Loo JSC. Toxicity of zinc oxide (ZnO) nanoparticles on human bronchial epithelial cells (BEAS-2B) is accentuated by oxidative stress. Food Chem Toxicol. 2010; 48:1762–1766. [PubMed: 20412830]
29. Pan ZW, Tao J, Zhu YM, Huang JF, Paranthaman MP. Spontaneous growth of ZnCO3 nanowires on ZnO nanostructures in normal ambient environment: Unstable ZnO nanostructures. Chem Mater. 2010; 22:149–154.
30. Crocket JH. Coprecipitation of zinc with calcium carbonate. Geochimica et Cosmochimica Acta. 1966; 30
31. Cedervall T, Lynch I, Lindman S, Berggard T, Thulin E, Nilsson H, Dawson KA, Linse S. Understanding the nanoparticle-protein corona using methods to quantify exchange rates and

affinities of proteins for nanoparticles. Proc Natl Acad Sci U S A. 2007; 104:2050–2055. [PubMed: 17267609]

32. Dell'orco D, Lundqvist M, Oslakovic C, Cedervall T, Linse S. Modeling the time evolution of the nanoparticle-protein corona in a body fluid. Public Library of Science. 2010; 5:e10949.
33. Faunce TA, White J, Matthaei KI. Integrated research into the nanoparticle-protein corona: a new focus for safe, sustainable and equitable development of nanomedicines. Nanomedicine (Lond). 2008; 3:859–866. [PubMed: 19025459]
34. Lundqvist M, Stigler J, Elia G, Lynch I, Cedervall T, Dawson KA. Nanoparticle size and surface properties determine the protein corona with possible implications for biological impacts. Proc Natl Acad Sci U S A. 2008; 105:14265–14270. [PubMed: 18809927]
35. Zydney ALHC. Effect of membrane morphology on the initial rate of protein fouling during microfiltration. J Memb Sci. 1999; 155:15.
36. Ostojic S. A DSC study of zinc binding to bovine serum albumin (BSA). J Serb Chem Soc. 2007; 72:7.
37. Oberdorster G. Lung particle overload: implications for occupational exposures to particles. Regul Toxicol Pharmacol. 1995; 21:123–135. [PubMed: 7784625]
38. Geiser M, Rothen-Rutishauser B, Kapp N, Schurch S, Kreyling W, Schulz H, Semmler M, Im Hof V, Heyder J, Gehr P. Ultrafine particles cross cellular membranes by nonphagocytic mechanisms in lungs and in cultured cells. Environ Health Perspect. 2005; 113:1555–1560. [PubMed: 16263511]
39. Handbook of Chemistry and Physics. 45. Chemical Rubber Company; Cleveland, OH: 1965.
40. Liu J, Aruguete DM, Murayama M, Hochella MF Jr. Influence of size and aggregation on the reactivity of an environmentally and industrially relevant nanomaterial (PbS). Environ Sci Technol. 2009; 43:8178–8183. [PubMed: 19924941]

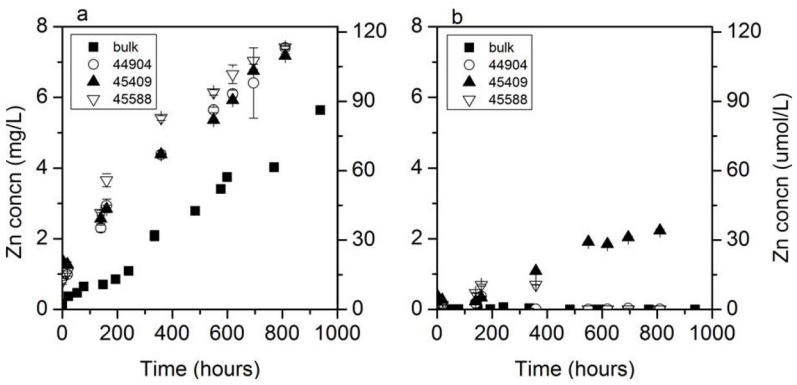

Figure 1.

Long-term dissolution of 100 mg/L bulk and nano ZnO (Alfa Aesar 44904, 45409, and 45588) in nanopure water (**a**) and moderately hard water (**b**). Y-axis for all graphs is Zn concentration in filtrate. Error bars are 95% confidence intervals.

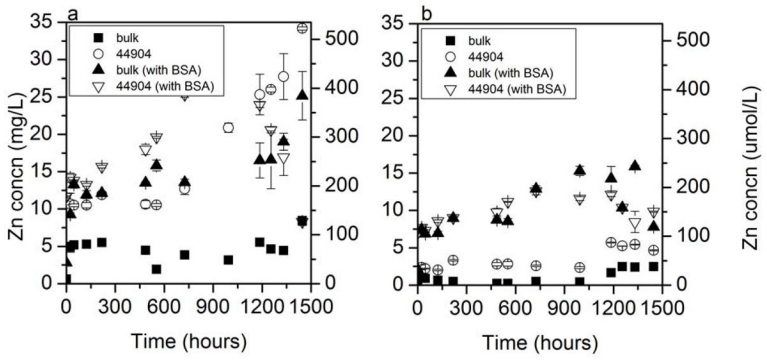

Figure 2.

Long-term dissolution of 100 mg/L bulk and nano ZnO (Alfa Aesar 44904) in Dulbecco's Modified Eagle's Medium (DMEM) (**a**) and Roswell Park Memorial Institute medium (RPMI) (**b**) (each with and without 2 mg/ml bovine serum albumin [BSA]). Y-axis for all graphs is Zn concentration in filtrate. Error bars are 95% confidence intervals.

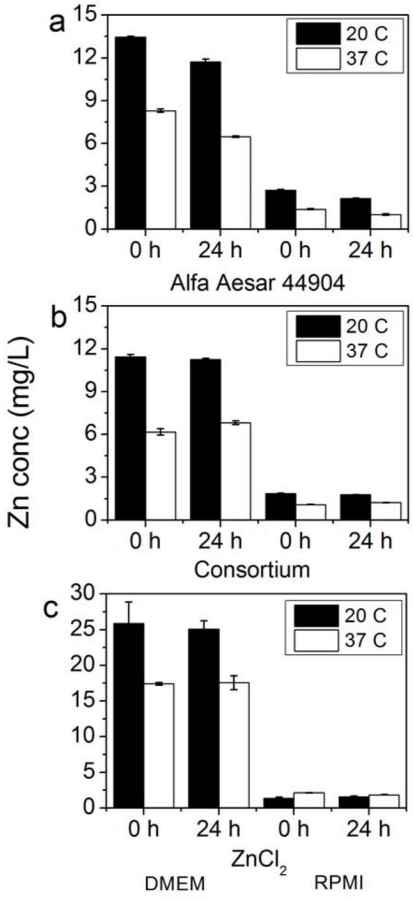

Figure 3.

Dissolution of 100 mg/L ZnO NPs (Alfa Aesar 44904, consortium) in Dulbecco's Modified Eagle's Medium (DMEM) and Roswell Park Memorial Institute medium (RPMI) after 0 and 24 h at both 20°C and 37°C. A dissolved zinc control (100 mg/L Zn from $ZnCl_2$) was also used to test for Zn precipitates in these cell culture matrices. Y-axis for all graphs is Zn concentration in filtrate.

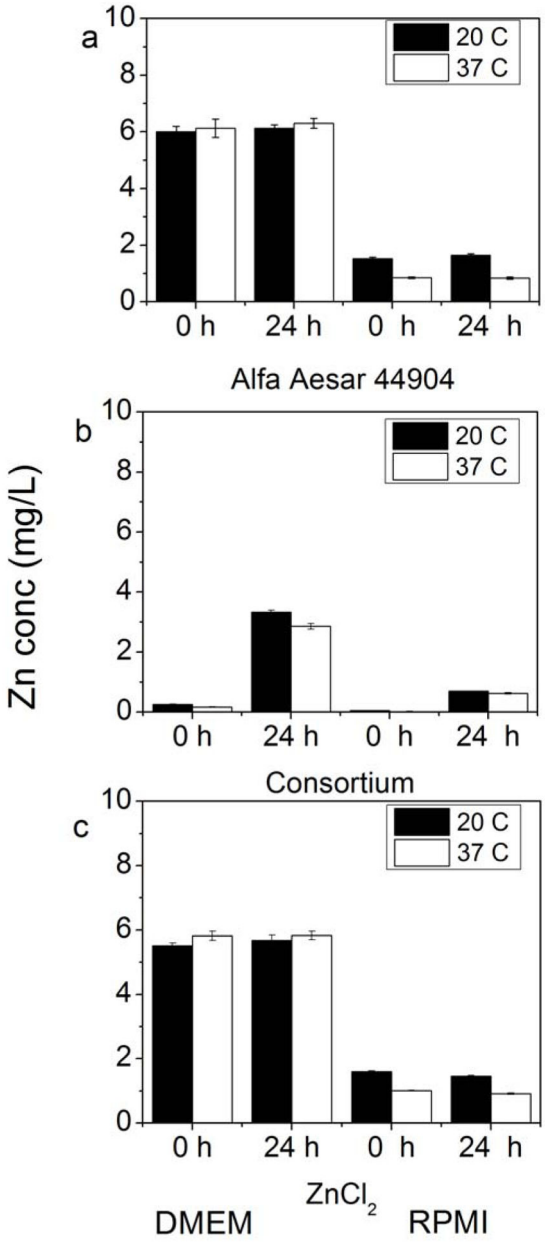

Figure 4.

Dissolution of 10 mg/L ZnO NPs (Alfa Aesar 44904, consortium) in Dulbecco's Modified Eagle's Medium (DMEM) and Roswell Park Memorial Institute medium (RPMI) after 0 and 24 h at both 20°C and 37°C. A dissolved zinc control ($ZnCl_2$) was also used to test for Zn precipitates in these cell culture matrices. Y-axis for all graphs is Zn concentration in filtrate.

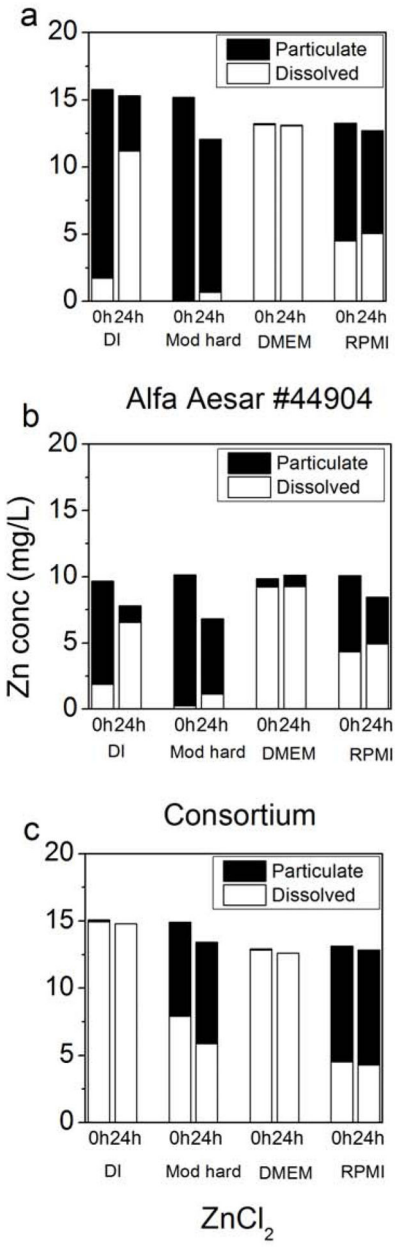

Figure 5.

Particulate and dissolved zinc concentrations in various matrices at 20°C after 0 and 24 h using ~10 mg/L Alfa Aesar 44904 (**a**) and consortium ZnO (**b**) NPs. $ZnCl_2$ (**c**) was used as a dissolved zinc control to test for possible Zn precipitation in solution. Dissolved concentration was measured directly in the filter permeate; particulate concentration is calculated as ($[Zn]_{feed}$-$[Zn]_{permeate}$.) Total column height (black + white) represents measured feed Zn concentration.

Table 1

Characterization of bulk and nanoparticulate ZnO by scanning electron microscopy, dynamic light scattering, and zeta potential measurements[a]

	Manufacturer's reported size (nm)	Morphology SEM[b]	Size by DLS[c] (nm), *n* = 3	Surface charge by zeta at pH ~8 (mV), *n* = 2
Bulk	-	Irregular	1920±151	−14.8±1.2
Alfa Aesar 44904	70	Irregular Angular	274±8	−18.5±1.2
Alfa Aesar 45409	40	Rounded	159±4	−21.6±3.7
Alfa Aesar 45588	70	Angular	179±3	−23.4±3.1
Consortium	25	Spheroid	215±15	−29.2±1.0

[a]The Alfa Aesar nanoparticles (NPs) were observed to have highly polydisperse size distributions by SEM and are, on average, the primary particle size reported by the manufacturer. Error in DLS and zeta potential values is the standard deviation of the mean values reported by the instrument. Additional analysis of all five particles by X-ray diffraction confirmed materials as ZnO (Zincite).

[b]SEM = Scanning electron microscopy.

[c]DLS = Dynamic light scattering.